



Journal of Applied and Computational Mechanics



Research Paper

Precision Shape Control of Ultra-thin Shells with Strain Actuators

Kainan Wang¹, David Alaluf², Gonçalo Rodrigues², André Preumont¹

¹ Department of Control Engineering and System Analysis, Université Libre de Bruxelles (ULB),
CP. 165-55, 50 Av. F.D. Roosevelt, B-1050 Brussels, Belgium, Emails: kainan.wang@ulb.ac.be, andre.preumont@ulb.ac.be

² European Space Agency—ESA/ESTEC Keplerlaan 1, 2201 AZ Noordwijk ZH, The Netherlands, Emails: david.alaluf@esa.int, goncalo.rodrigues@esa.int

Received January 10 2020; Revised June 02 2020; Accepted for publication June 02 2020.

Corresponding author: André Preumont (andre.preumont@ulb.ac.be)

© 2021 Published by Shahid Chamran University of Ahvaz

Abstract. This paper is part of an effort conducted at Université libre de Bruxelles (ULB) on behalf of European Space Agency (ESA) to control the shape of thin polymer shell structures with a unimorph layer of strain actuators (Polyvinylidene fluoride-co-trifluoroethylene, PVDF-TrFE), to achieve high quality light-weight foldable reflectors for space observation. The paper discusses the influence of the electrode size on the morphing capability of the system and addresses the difficulty associated with the ill-conditioning when controlling a very large set of electrodes. The final part of the paper describes a technology demonstrator currently under development and presents some simulation results fitting low order optical modes.

Keywords: Adaptive Shell, Polymer Composite, Piezoelectric Actuator, PVDF, Space Telescope, Shape control.

1. Introduction

Currently, the *James Webb Space Telescope* (JWST) is the largest space telescope; its primary mirror consists of 18 hexagonal segments made of Beryllium for a total diameter of 6.5 m; its areal density is 20 kg/m². The foldable primary mirror is actively controlled for cancelling the deployment errors and the orbital disturbances. After several delays, JWST is supposed to be launched in Spring 2021, for a total estimated cost of 10 Billion USD. It will be operated at the Lagrange point L2 in the infrared (λ from 0.6 to 28 μ m).

The present study is motivated by the need for even larger and lighter space reflectors with a diameter of 10 m and more, to provide sufficient collecting area to feed spectrographs and other sensing equipment. The difficulty comes from the tight weight and volume constraints (requiring foldable reflectors), the harsh vibratory environment during the launch and the tight surface figure accuracy ($\lambda/14$). The space community is looking for a new paradigm of foldable reflectors with an areal density of 3 kg/m² or less. Two options may be considered: (i) inflatable membranes and (ii) shape stiffened shells. Lenticular membrane reflectors (Fig. 1.a) are made of two circular plane membranes glued to each other on the edge; one of them is covered with a reflecting material on the inside and will form the reflector, while the other is transparent and will form the canopy. The focal length can be adjusted by the internal pressure. The wavefront error of lenticular structures tends to be dominated by the spherical aberration [1] which is difficult to cancel by active means. Besides, inflatable structures are prone to gas leakage due to micro-meteorites. The second option is investigated here; it consists of a polymer elastic shell molded in its final shape and rolled for stowage; once released in orbit, the reflector unfolds on its own strain energy (Fig. 1.b) [2, 3]. Note that, besides the high accuracy imaging reflectors, there are less stringent applications such as LIDAR (Light Detection and Ranging), laser communication and light collectors for spectroscopy.

The paper is organized as follows: The first part discusses the strain actuation of a spherical shell and highlights the fundamental difference with respect to a plate. It also discusses the connection between the electrode size and the optical quality; good optical performances with small focal length will require a large number of electrodes. The second part addresses the difficulty associated with the ill-conditioning of the Jacobian when controlling a large array of electrodes; a hierarchical approach is proposed, based on Saint-Venant's principle. The third part of the paper describes a small-scale technology demonstrator under development and presents some simulation results illustrating its morphing capability for low order optical (Zernike) modes.

2. Strain Actuated Spherical Shell

Strain actuators constitute a very efficient way of controlling flat plates; piezoelectric ceramic operating in d_{31} mode¹ have proved very effective in adaptive optics (AO). A patch of isotropic ($d_{31} = d_{32}$) piezoelectric material acting on a plate may be modelled by a set of equivalent forces consisting of an in-plane force normal to the contour of the electrode, and a constant moment acting on the contour of the electrode [4] (see Fig. 2). The force and moment per unit length are respectively

$$N_p = e_{31}V \quad M_p = e_{31}Vz_m \quad (1)$$

¹ The piezoelectric layer is expanded horizontally when applying a vertical electric field.



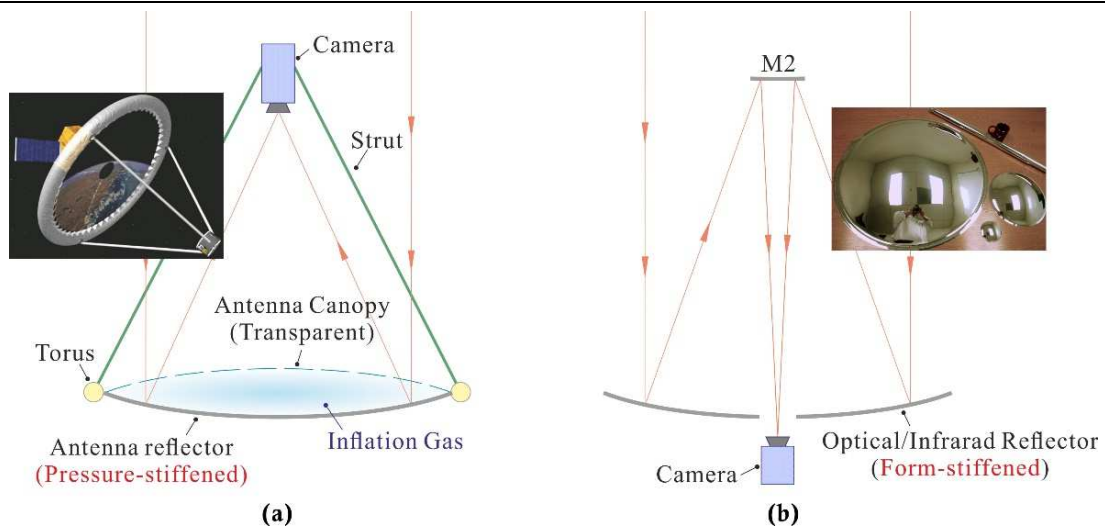


Fig. 1. (a) Lenticular membrane reflector (source: NASA). (b) Polyimide thin shell reflector in deployed and rolled configurations (source: MEVICON).

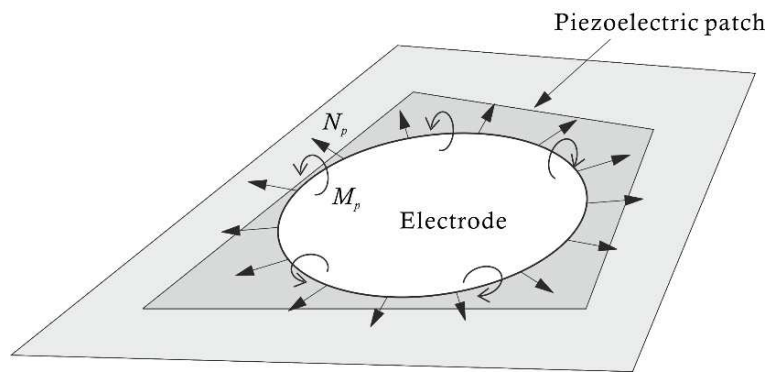


Fig. 2. Equivalent piezoelectric loads (per unit length) for an isotropic piezoelectric actuator: $N_p = e_{31}V$, $M_p = e_{31}z_mV$.

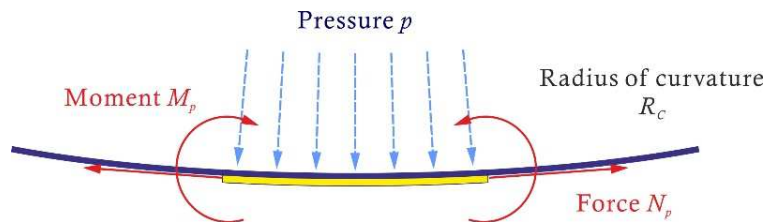


Fig. 3. Equivalent piezoelectric loads (per unit length) for an isotropic piezoelectric actuator on a sphere: $N_p = e_{31}V$, $M_p = e_{31}z_mV$ and $p = 2N_p/R_c$.

where $e_{31} = d_{31}E_p/(1-\nu_p)$, d_{31} is the in-plane piezoelectric constant; it may be positive (e.g. PVDF) or negative (e.g. PZT); E_p and ν_p are the Young modulus and the Poisson's ratio of the piezoelectric material, V the voltage difference applied to the electrodes and z_m is the distance between the mid plane of the substrate and that of the piezoelectric layer. Note that the strain actuation forces being internal forces, they are always self-equilibrated.

If the structure is a spherical shell and if the force N_p normal to the contour acts in the tangent plane, the foregoing set of forces is no longer self-equilibrated; it must be supplemented by a uniform pressure p acting normally to the electrode to balance the normal component of the force N_p acting on the contour of the electrode [5] (see Fig. 3):

$$p = \frac{2N_p}{R_c} \tag{2}$$

where R_c is the radius of curvature of the shell substrate.

The foregoing equivalent loads apply when the piezoelectric properties of the material are isotropic in plane ($d_{31} = d_{32}$) and the shell is a sphere. In more general situations, the piezoelectric actuation can be modelled by finite elements (FE) using the thermal equivalence, since both piezoelectric actuation in d_{31} mode and the planar thermal expansion behave identically

$$d_{31}V/t_p = \Delta\alpha \Delta T \tag{3}$$

where t_p is the thickness of the piezoelectric material (V/t_p is the electric field) and $\Delta\alpha$ is the difference of thermal expansion coefficient (CTE) between the substrate and the piezoelectric layer, and ΔT is the temperature change applied to the system. A numerical comparison conducted with the FE software SAMCEF confirms the good agreement between the equivalent forces, the thermal model and the full piezoelectric model [6].



Table 1. Material parameters for the simulation.

	PET	PVDF
Young's modulus [GPa]	5.6	2.5
Poisson's ratio []	0.38	0.34
Dielectric constant []	-	10
Piezoelectric constant d_{31} [pC/N]	-	15
Max. Electric Field (V/mm)	15×10^5	5×10^5
Thermal expansion CTE ($10^{-6}K^{-1}$)	59.4	140-128

In order to analyze the influence of the curvature on the mechanical behavior of a spherical shell subject to piezoelectric actuation, consider the structure of Fig. 4 made of Polyethylene terephthalate (PET); the diameter is $D = 200$ mm, the thickness is $t = 100$ μm ; it is clamped on the edge and covered by a layer of 5 μm of PVDF-TrFE with a central electrode of diameter $D_a = 50$ mm; a voltage difference $V = 10$ V is applied. The material properties are reported in Tab. 1. Figure 4 shows the evolution of the deformation when the radius of curvature R_c is reduced from 50 m (nearly flat) to 0.5 m. The computations are performed with the piezoelectric module of SAMCEF.

The radius of curvature R_c is related to the focal length f of the reflector according to $f = R_c/2$. In Fig. 4, one sees that when the shell is nearly flat [$R_c = 50$ m, $D_a/(R_c t)^{1/2} = 0.7$], the deformations are very similar to that of a flat plate. On the contrary, for $R_c = 0.5$ m, $D_a/(R_c t)^{1/2} = 7$, the shell deformations appear as the footprint of the electrode (note that the amplitude is also significantly reduced). The surface of the reflector exhibits a quick transition region of $\rho = (R_c t)^{1/2}$ at the edge of the electrode. For a reflector equipped with an electrode array, this rapid change in the surface figure may be a source of a significant wavefront error [7], unless the characteristic length of the electrodes, D_e is such that

$$D_e < (R_c t)^{1/2} \tag{4}$$

This constraint is fairly stringent for thin reflectors of short focal length. For example, a reflector of thickness $t = 175$ μm with a diameter $D = 10$ m and a radius of curvature $R_c = 200$ m would require more than $N = 2000$ independent electrodes, while the same reflector with $R_c = 20$ m would require 10 times more.

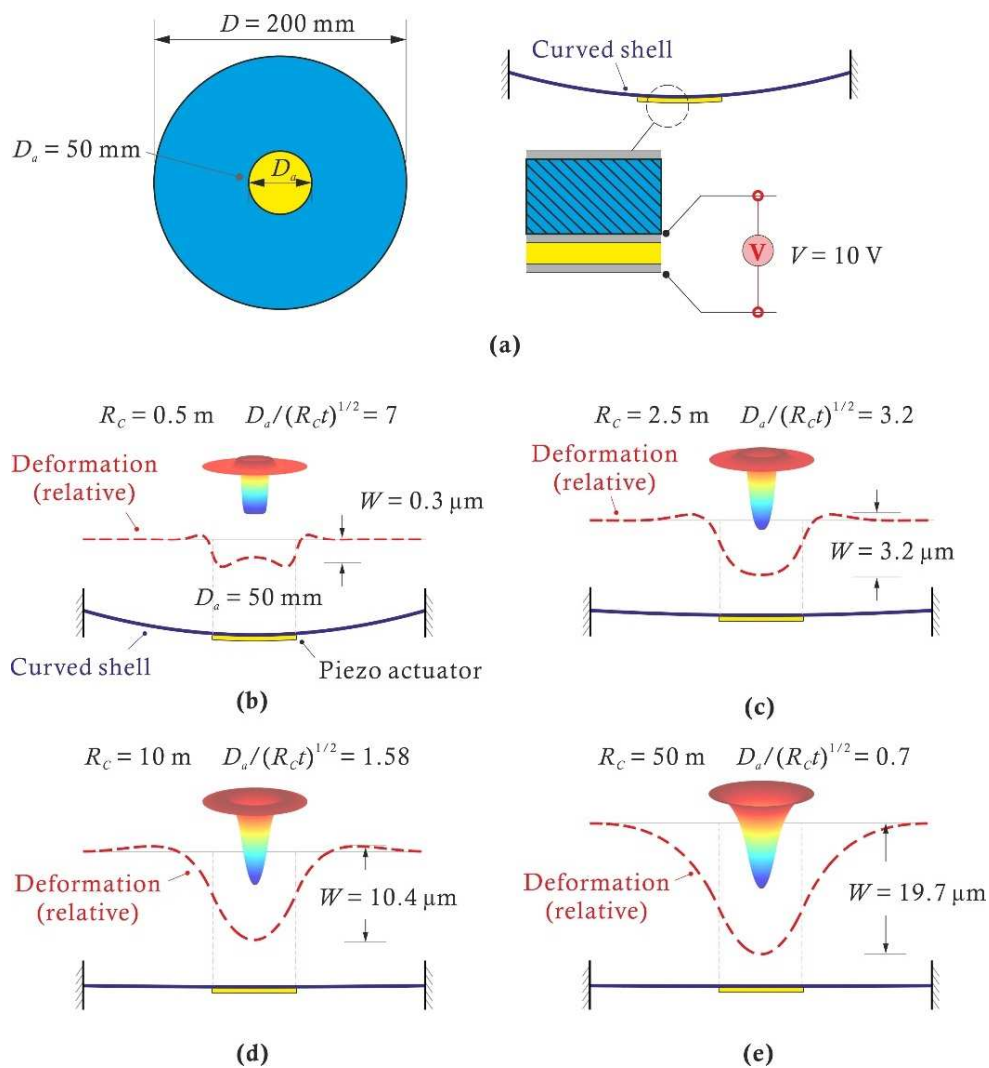


Fig. 4. Influence of the radius of curvature R_c on the deformation of a clamped piezoelectric spherical shell actuated by a central electrode.



3. Shape Control

The control aims at compensating the manufacturing errors, the possible creep in rolled configuration as well as all disturbances of orbital origin, such as the thermal gradient and the gravity gradient; all of these are slow, so that the problem is quasi-static. Assuming a linear behavior for small perturbations, the vector of surface figure sensor error \mathbf{s} (whatever sensor is used) and the vector of applied electrode voltages \mathbf{v} are related by a rectangular matrix, the Jacobian:

$$\mathbf{s} = \mathbf{J}\mathbf{v} \tag{5}$$

Thus, once known the requested displacements, the voltage map may be obtained by

$$\mathbf{v} = \mathbf{J}^+\mathbf{s} \tag{6}$$

where \mathbf{J}^+ is the pseudo-inverse of the Jacobian. This can be done by Singular Value Decomposition (SVD). However, when the electrode size becomes very small and their number very large, the ill-conditioning of the Jacobian resulting of the weak authority of individual electrodes, cannot be resolved easily by classical regularization methods [8]. In this case, a hierarchical approach may be used, based on Saint-Venant's principle: *the difference between the effects of two different, but statically equivalent loads becomes very small at sufficiently large distances from the loads*. This suggests that the small electrodes can be grouped in macro electrodes and that small variations within one macro electrode will not affect significantly the surface figure outside this macro electrode. The control algorithm is decomposed into a global control phase in which the voltages of the macro electrodes are adjusted to minimize the global sensor error, followed by a local control phase in which the local voltages of the small electrodes are adjusted iteratively in order to minimize the remaining surface figure error (local sensor) within every macro electrode (Fig. 5). The grouping of electrodes should be done in such a way that the aspect ratio² of the macro electrodes is close to 1. Numerical simulations [9] show that: (i) The Gauss-Seidel iteration normally presents better convergence performances than the Jacobi iteration; (ii) the spectral radius (defined as the largest absolute value of matrix eigenvalues, which must be lower than 1 for convergence) tends to increase with the number of macro electrodes (which means that the convergence is slower); (iii) frequent execution of the global control problem will increase the convergence within intervals of local shape control.

4. MATS demonstrator

This section describes briefly a small-scale technology demonstration project called *Multilayer Adaptive Thin Shell Reflectors for Future Space Telescopes* (MATS) developed on behalf of ESA in the framework of the General Support Technology Programme (GSTP) program. The project aims at developing the technology and demonstrating the feasibility on a small-scale test article (to validate the unimorph actuation of piezoelectric layer on curved surfaces); it is conducted in collaboration with the research center MateriaNova which is taking care of all the materials aspects.

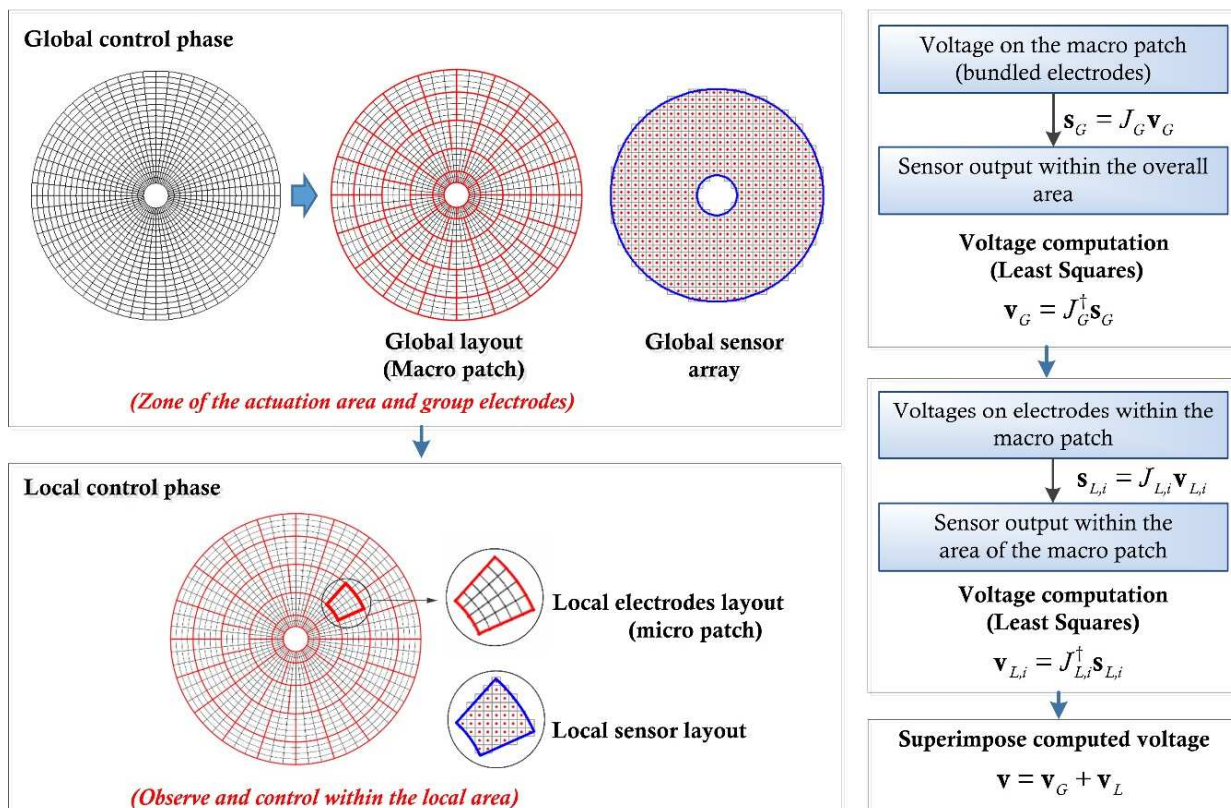


Fig. 5. Hierarchical control of a large electrode array. \mathbf{s}_G is the output vector of the global sensor; \mathbf{v}_G is the computed vector of voltages of the macro electrodes. $\mathbf{s}_{L,i}$ is the sensor output and $\mathbf{v}_{L,i}$ is the computed vector of voltage of the individual electrodes within the macro electrode i .

² The aspect ratio can be generally defined as $L_p/4S_a^{1/2}$, where L_p is the perimeter and S_a is the area of the macro electrode.



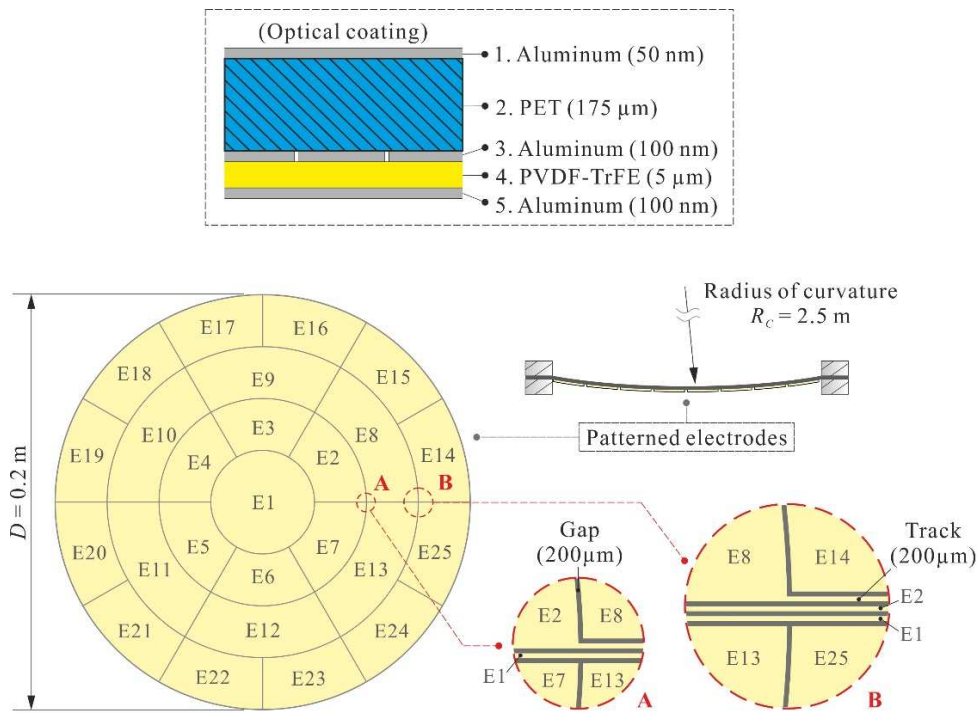


Fig. 6. MATS demonstrator. Top: Cross section showing the layer sequence. Bottom: Geometry of the 25 control electrodes with a keystone layout. The pattern includes tracks of 200 μm width, separated with 200 μm gaps, to connect the electrodes in the interior part of the reflector to the rim.

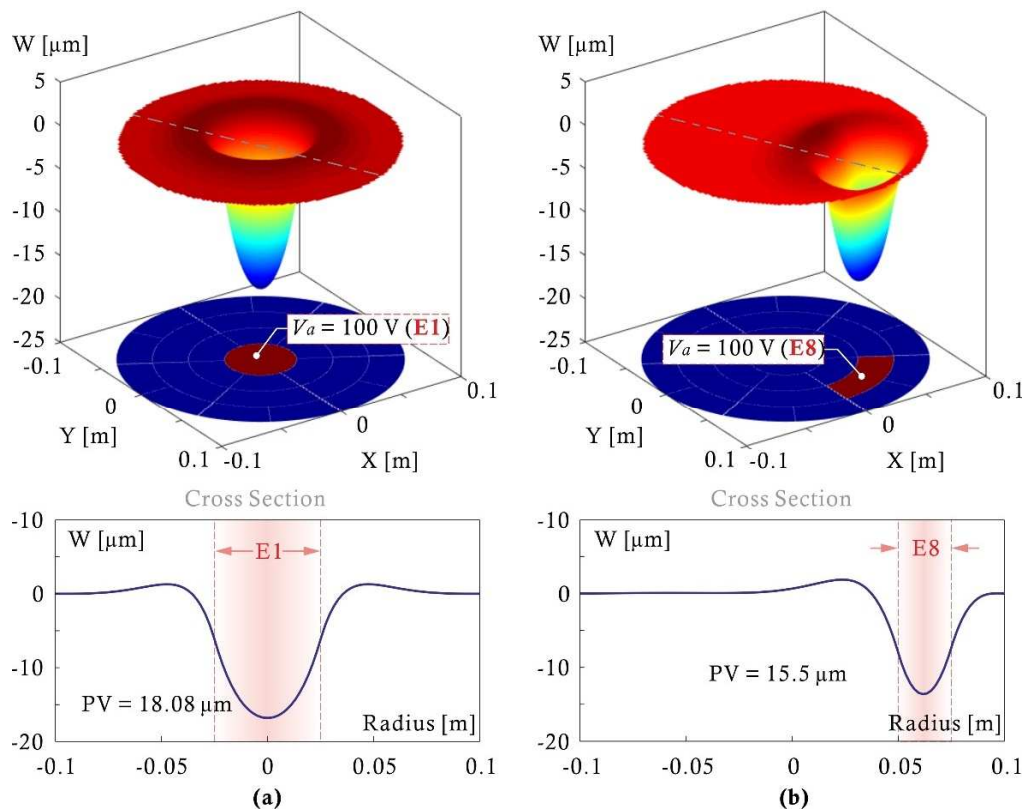


Fig. 7. MATS demonstrator. Influence functions of control electrodes E1 and E8 when a voltage difference of 100 V is applied.

The test article consists of a spherical shell of diameter 200 mm made of PET with a thickness $t = 175$ μm and a radius of curvature $R_c = 2.5$ m. The front side is a reflecting Aluminum layer of 50 nm while the back side is covered with a patterned Aluminum electrode of 100 nm, an active layer of PVDF-TrFE of 5 μm and a ground electrode of 100 nm; the patterned electrode consists of 25 independent electrodes with a keystone layout (Fig. 6). The considerations relative to manufacturing of the spherical substrate, the thin film deposition and the electrostrictive behavior of the PVDF-TrFE will be addressed in a subsequent publication; this paper assumes a linear piezoelectric behavior and focuses on the numerical prediction of the performance of the control system. Notice that the radial width of the electrodes is 25 mm, close to the transition critical length $\rho = (R_c t)^{1/2} \sim 21$ mm discussed above. The electrodes are connected to the rim of the structure by tracks of 200 μm width, separated with gaps of 200 μm, and from the rim to the control electronics, outside the useful part of the reflector. Note that the patterned electrode is trapped between the PET



substrate and the active PVDF-TrFE layer, to avoid arcing. The simulation results reported in the following section have been obtained with the piezoelectric module of SAMCEF [6] with the material properties of Tab. 1 and the geometry of Fig. 6. The FE model includes the tracks and the gaps necessary for the electrical connection of the electrodes distant from the periphery of the reflector. The piezoelectric constant $d_{31} = 15$ pC/N was obtained experimentally.

5. Simulation Results

Figure 7 shows the influence functions of two control electrodes, the central one E1 and electrode E8 when a voltage difference of 100 V is applied; the figure also includes a cross section of the normal displacements W . Figure 8 to 11 shows the reflector shape and the voltage map for typical optical modes (respectively *defocus* Z_4^3 , *astigmatism* Z_5 , *trefoil* Z_6 and *coma* Z_7) normalized to a peak to valley (PV) amplitude (10 or 5 μm) in a central pupil of 120 mm diameter. The RMS figure errors are also reported on the figures. The voltage map is computed in order to minimize the RMS figure error between the targeted optical mode and the actual shape of the reflector within the pupil of 120 mm. These results assume that the sensor measures the vertical displacement over the whole pupil (the Jacobian J is expressed in m/V). All results are based on the pseudo-inverse J^+ , except for the astigmatism of Fig. 9 where the method of *damped least squares* [8] has been used to compute the voltages required to compensate the figure error, with $\alpha_{DLS} = 5 \times 10^{-8}$ in order to reduce the voltage range without increasing significantly the residual figure error.

6. Conclusions

The precision shape control of ultra-thin spherical shells with distributed piezoelectric strain actuators has been analyzed. It has been shown that, in order to achieve a precise shape, it is necessary to use independent electrodes not larger than a characteristic length related to the radius of curvature R_c and the shell thickness t according to $D_e \leq (R_c t)^{1/2}$. For large and thin reflectors, this geometrical constraint requires a large electrode array, leading to ill-conditioning in the Jacobian. A hierarchical approach has been outlined, which combines iteratively a global and a local control phase. Finally, a small-scale technology demonstrator has been described and numerical finite element simulations have been presented.

Ongoing additional researches include the material characterization of the PVDF-TrFE (in particular its poling strain and its electrostrictive behavior), the manufacturing of the demonstrator and the metrology to evaluate the performance of the system. All these aspects will be reported in future publications.

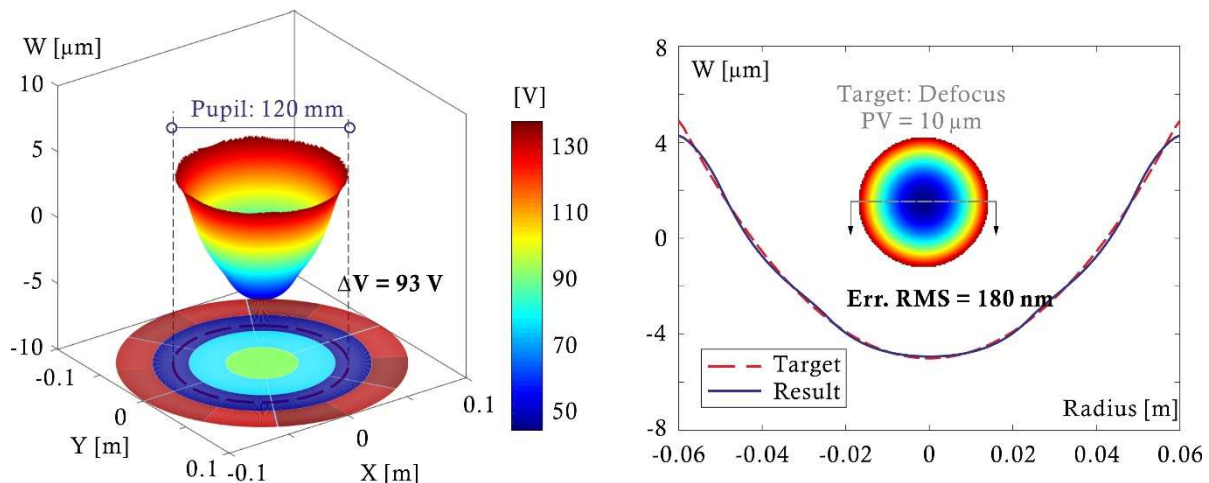


Fig. 8. MATS demonstrator. Defocus mode with a PV amplitude of 10 μm . Best fit reflector shape and voltage map for a pupil of 120 mm.

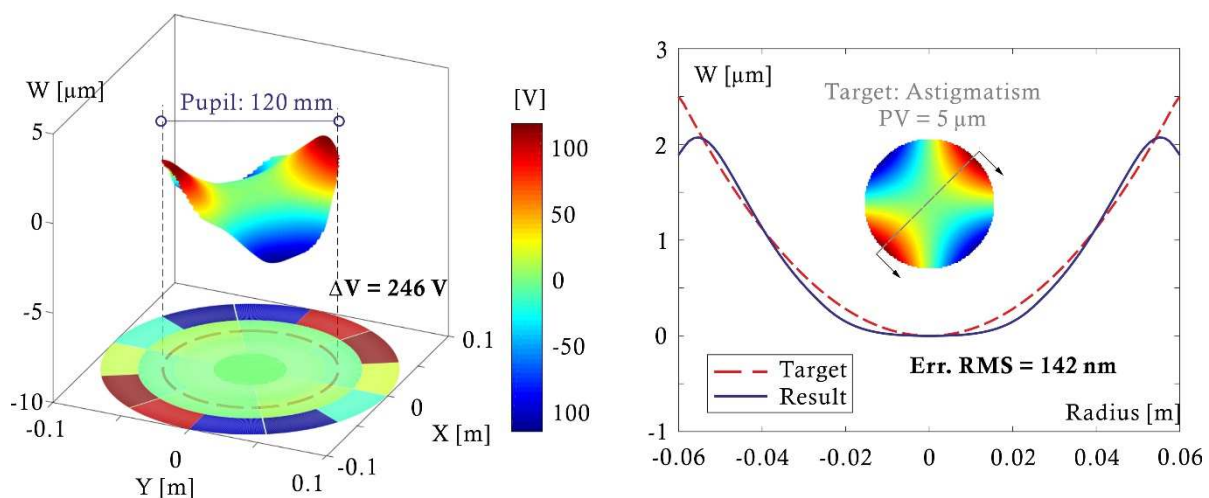


Fig. 9. MATS demonstrator. Astigmatism mode with a PV amplitude of 5 μm . Best fit reflector shape and voltage map for a pupil of 120 mm.

³ according to Noll's ordering of the Zernike modes.



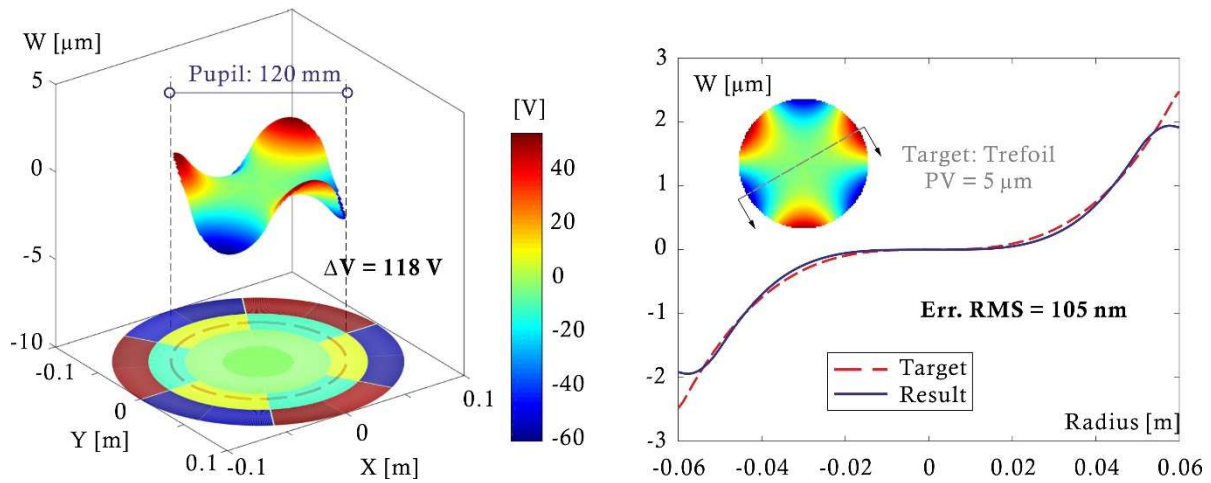


Fig. 10. MATS demonstrator. Trefoil mode with a PV amplitude of 5 μm. Best fit reflector shape and voltage map for a pupil of 120 mm.

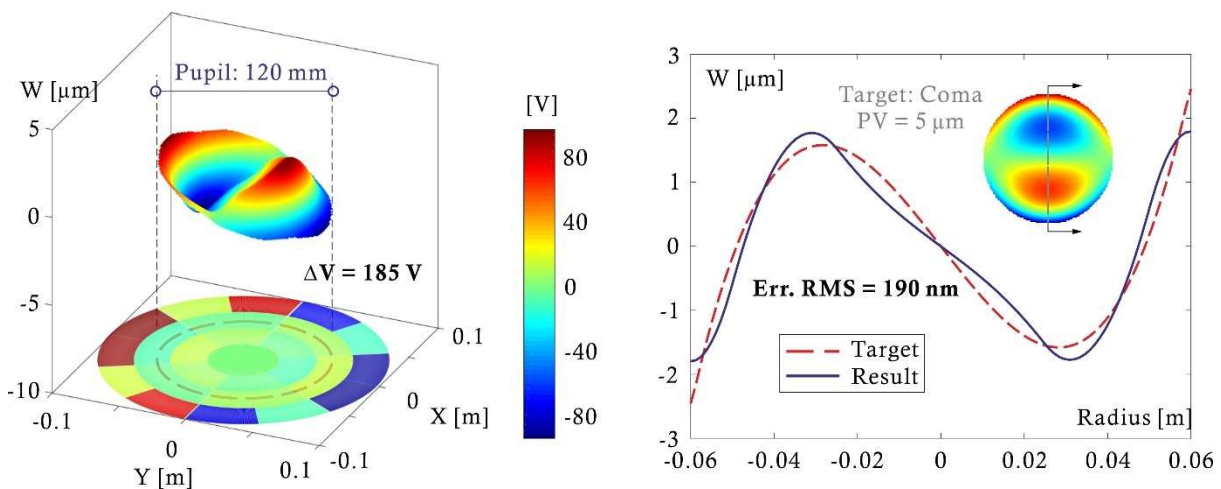


Fig. 11. MATS demonstrator. Coma mode with a PV amplitude of 5 μm. Best fit reflector shape and voltage map for a pupil of 120 mm.

Author Contributions

A. Preumont and G. Rodrigues planned the scheme, initiated the project and suggested the experiments; K. Wang and D. Alaluf conducted the experiments and analyzed the empirical results; K. Wang and D. Alaluf developed the mathematical modeling and examined the theory validation. The manuscript was written through the contribution of all authors. All authors discussed the results, reviewed and approved the final version of the manuscript.

Acknowledgments

The authors wish to thank their colleagues Thomas Godfroid and Damien Robert from MateriaNova who are preparing the demonstrator that will be used in the experimental part of this project.

Conflict of Interest

The authors declared no potential conflicts of interest with respect to the research, authorship and publication of this article.

Funding

This project is funded by the European Space Agency (ESA) in the framework of the GSTP program, project *Multilayer Adaptive Thin Shell for Future Space Telescopes* (MATS - RFQ 3-14210/14/PA/NL).

Nomenclature

N_p	Equivalent force per unit length [N/m]	D_a	Diameter of the central electrode [m]
M_p	Equivalent moment per unit length [N]	D_e	Characteristic length of the electrode [m]
d_{31}, d_{32}	In-plane piezoelectric constant [C/N or V/m]	ρ	Characteristic length of the reflector $\rho = (Rct)^{1/2}$ [m]
E_p	Young modulus of the piezoelectric material [Pa]	\mathbf{s}	Vector of surface figure sensor error [m]
ν_p	Poisson's ratio of the piezoelectric material []	\mathbf{v}	Vector of applied electrode voltages [V]
V	Voltage difference applied to the electrodes [V]	J	Interaction matrix of the system, Jacobian [m/V]
z_m	Distance between the mid plane of the substrate and	J^+	Pseudo-inverse of the Jacobian [V/m]





	that of the piezoelectric layer [m]		
p	Equivalent uniform pressure acting normally to the electrode to balance the normal component of the force [Pa]	\mathbf{s}_G	Output vector of the global sensor [m]
R_c	Radius of curvature of the shell substrate [m]	\mathbf{v}_G	Vector of voltages of the macro electrodes [V]
t_p	Thickness of the piezoelectric material [Pa]	$\mathbf{s}_{L,i}$	Sensor output of the individual electrodes within the macro electrode i [m]
α	Thermal expansion coefficient (CTE) [K ⁻¹]	$\mathbf{v}_{L,i}$	Vector of voltage of the individual electrodes within the macro electrode i [V]
T	Temperature change applied to the system [K]	t	Thickness of the reflector substrate [m]
D	Diameter of the reflector [m]	α_{DLS}	Damping coefficient of DLS algorithm [/]


References

- [1] Marker, D.K., Jenkins, C.H., Surface Precision of Optical Membranes with Curvature, *Optics Express*, 1(11), 1997, 324-331.
- [2] Flint, E., Bales, G., Glaese, R., Bradford, R., Experimentally Characterizing the Dynamics of 0.5 m Diameter Doubly Curved Shells Made from Thin Films, 44th AIAA/ASME/ASCE/AHS/ASC Structures, Structural Dynamics, and Materials Conference, AIAA Paper 2003-1831, Norfolk, Virginia, USA, p. 1831, 2003.
- [3] Flint, E., Lindler, J., Hall, J., Rankine, C., Regelbrugge, M., Overview of Form Stiffened Thin Film Shell Characteristic Behavior, 47th AIAA/ASME/ASCE/AHS/ASC Structures, Structural Dynamics, and Materials Conference, Newport, Rhode Island, USA, p. 1900, 2006.
- [4] Preumont, A., *Vibration Control of Active Structures, An Introduction, 4th Edition*, Springer International Publishing, 2018.
- [5] Chaudhry, Z., Lalande, F. and Rogers, C.A., Modeling of Induced Strain Actuation of Shell Structures, *Journal of the Acoustical Society of America*, 97(5), 1995, 2872-2877.
- [6] Piefort, V., Loix, N., Preumont, A., Modeling of Piezolaminated Composite Shells for Vibration Control, *ESA Conference on Spacecraft Structures, Materials and Mechanical Testing*, Braunschweig, Germany, ESA SP-428, 1998.
- [7] Preumont, A., Alaluf, D., Wang, K. and Rodrigues, G. Adaptive Thin Shell Reflectors for Future Space Telescopes, 14th European Conference on Spacecraft Structures, Materials and Environmental Testing (ECSSMET 2016), Toulouse, France, September 2016.
- [8] Buss, S.R., Introduction to Inverse Kinematics with Jacobian Transpose, Pseudoinverse and Damped Least-Squares Methods, *IEEE Journal of Robotics and Automation*, 17(1-19), 2004, 16.
- [9] Wang, K., *Piezoelectric Adaptive Mirrors for Ground-based and Space Telescopes*, Ph. D Thesis, Active Structures Laboratory, Université Libre de Bruxelles, Brussels, Belgium, 2019.

ORCID iD

Kainan Wang  <https://orcid.org/0000-0003-0914-4513>

Gonçalo Rodrigues  <https://orcid.org/0000-0001-5072-0821>

André Preumont  <https://orcid.org/0000-0003-2632-177X>



© 2021 Shahid Chamran University of Ahvaz, Ahvaz, Iran. This article is an open access article distributed under the terms and conditions of the Creative Commons Attribution-NonCommercial 4.0 International (CC BY-NC 4.0 license) (<http://creativecommons.org/licenses/by-nc/4.0/>).

How to cite this article: Wang K., Alaluf D., Rodrigues G., Preumont A. Precision Shape Control of Ultra-thin Shells with Strain Actuators, *J. Appl. Comput. Mech.*, 7(SI), 2021, 1130-1137. <https://doi.org/10.22055/JACM.2020.31899.1987>

